Facilitation versus depression in cultured hippocampal neurons determined by targeting of Ca^{2+} channel $Ca_v\beta_4$ versus $Ca_v\beta_2$ subunits to synaptic terminals

Mian Xie, Xiang Li, Jing Han, Daniel L. Vogt, Silke Wittemann, Melanie D. Mark, and Stefan Herlitze

Department of Neurosciences, Case Western Reserve University, Cleveland, OH 44106

Ca^{2+} channel β subunits determine the transport and physiological properties of high voltage–activated Ca^{2+} channel complexes. Our analysis of the distribution of the $Ca_v\beta$ subunit family members in hippocampal neurons correlates their synaptic distribution with their involvement in transmitter release. We find that exogenously expressed $Ca_v\beta_{4b}$ and $Ca_v\beta_{2a}$ subunits distribute in clusters and localize to synapses, whereas $Ca_v\beta_{1b}$ and $Ca_v\beta_3$ are homogenously distributed. According to their localization, $Ca_v\beta_{2a}$ and $Ca_v\beta_{4b}$ subunits modulate the synaptic plasticity of autaptic hippocampal neurons (i.e., $Ca_v\beta_{2a}$ induces depression, whereas $Ca_v\beta_{4b}$ induces paired-pulse facilitation [PPF] followed by synaptic depression during longer stimuli trains). The induction of PPF by $Ca_v\beta_{4b}$ correlates with a reduction in the release probability and cooperativity of the transmitter release. These results suggest that $Ca_v\beta$ subunits determine the gating properties of the presynaptic Ca^{2+} channels within the presynaptic terminal in a subunit-specific manner and may be involved in organization of the Ca^{2+} channel relative to the release machinery.

Introduction

High voltage–activated Ca^{2+} channels in neurons consist of several subunits, a pore-forming α_1 subunit ($Ca_v\alpha_1$), and several auxiliary subunits, including $\alpha_2\delta$ and β ($Ca_v\beta$; Catterall, 2000). $Ca_v\beta$ subunits are involved in transport of the pore-forming α_1 subunit to the plasma membrane (Dolphin, 2003; Herlitze et al., 2003). $Ca_v\beta$ subunits shield an ER retention signal on the α_1 subunit, thereby guiding the pore-forming subunit to the target membrane (Bichet et al., 2000).

$Ca_v\beta$ subunits also determine the biophysical properties of the Ca^{2+} channel. The effects of the $Ca_v\beta$ subunit family members on the biophysical properties are complex. Four family members have been described ($Ca_v\beta_{1–4}$). P/Q-type channels assembled with $Ca_v\beta_{1b}$ and β_3 subunits in heterologous expression systems are fast inactivating in comparison with $Ca_v\beta_4$- and β_2-assembled channels (Stea et al., 1994; Fellin et al., 2004; Luvisetto et al., 2004). $Ca_v\beta_2$ has the most dramatic effects on the channel properties, causing the channel to inactivate very slowly. In addition, the $Ca_v\beta_2$ subunit is unique because this subunit can be attached to the plasma membrane via its palmitoylated N-terminal protein domain (Chien et al., 1998).

Several studies also suggest that at least certain $Ca_v\beta$ subunit family members can target and function independently of the $Ca_v\alpha_1$ subunits at the plasma membrane and other intracellular structures such as the nucleus. For example, these subunits may be involved in gene transcription (Hibino et al., 2003) and the regulation of Ca^{2+} oscillations and insulin secretion (Berggren et al., 2004).

Recently, the crystal structures of the $Ca_v\beta$ core domains and the interaction domain between $Ca_v\beta$ and $Ca_v\alpha_1$ have been determined (Chen et al., 2004; Opatowsky et al., 2004; Van Petegem et al., 2004). These studies revealed that the $Ca_v\beta$ subunits belong to the membrane-associated guanylate kinase family containing Src homology type 3 and guanylate kinase domains (Hanlon et al., 1999; Richards et al., 2004; Rousset et al., 2005). A mutagenesis study of the Src homology type 3 and guanylate kinase domains showed that these domains regulate the inactivation of these Ca^{2+} channels (McGee et al., 2004) but also suggested that $Ca_v\beta$ subunits are involved in scaffolding and in the precise localization of Ca^{2+} channel complexes to defined subcellular domains. Indeed, deletion of the nonconserved N and C termini of the $Ca_v\beta_{4b}$ subunit results in a loss of synaptic localization and presynaptic function

Correspondence to Stefan Herlitze: sxh106@cwru.edu

Abbreviations used in this paper: AP, action potential; EPSC, excitatory postsynaptic current; PPF, paired-pulse facilitation; PPR, paired-pulse ratio; RRP, readily releasable vesicle pool; SFV, Semliki Forest virus.

The online version of this article contains supplemental material.

The Journal of Cell Biology, Vol. 178, No. 3, July 30, 2007 489–502
http://www.jcb.org/cgi/doi/10.1083/jcb.200702072

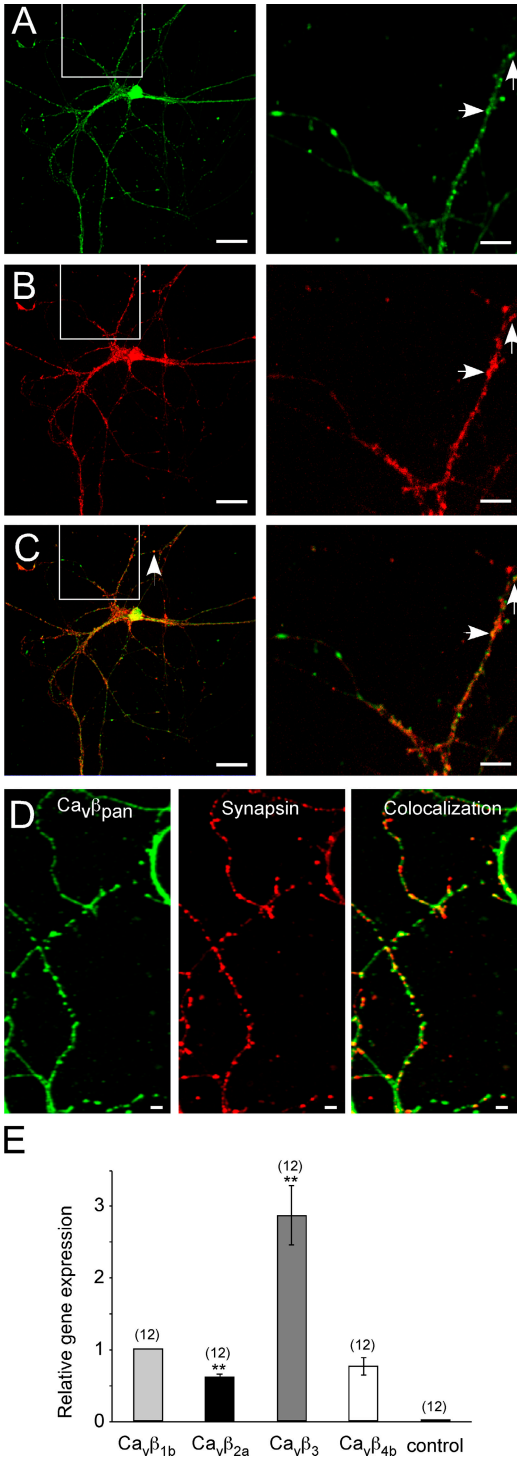

Figure 1. **Endogenous distribution and expression of $Ca_v\beta$ subunits in cultured hippocampal neurons.** (A–C) (A, green) Confocal pictures of the endogenous $Ca_v\beta$ subunits detected with a pan-β antibody reveal punctate staining. (B, red) Hippocampal neurons were stained with an anti–synaptobrevin-II antibody and visualized with an AlexaFluor546-coupled secondary antibody. (C) Overlay of A and B demonstrates that the endogenous $Ca_v\beta$ subunits are partially colocalized with the synaptic vesicle marker synaptobrevin-II. (right) Boxed areas show that several pan-staining puncta are colocalized with synaptobrevin-II (arrows). Magnification of the indicated areas from the neuron shown on the left. (D) $Ca_v\beta$ subunits colocalize with the synaptic marker synapsin-I. Confocal images of the endogenous $Ca_v\beta$ subunits in hippocampal neurons visualized with the pan-β antibody (left), synapsin-I visualized with an anti–synapsin-I antibody (middle), and overlay of the two pictures (right) reveal that endogenous $Ca_v\beta$ subunits partially colocalize with the presynaptic marker synapsin-I. (E) Endogenous $Ca_v\beta$ subunit mRNAs are expressed at different levels in cultured hippocampal neurons. The mRNA expression levels of $Ca_v\beta_{2a}$, $Ca_v\beta_3$, and $Ca_v\beta_{4b}$ were normalized to the mRNA level of the $Ca_v\beta_{1b}$ subunit. The bar graph shows that the $Ca_v\beta_3$ mRNA level was approximately three times higher than $Ca_v\beta_{1b}$, whereas the $Ca_v\beta_{2a}$ expression level was ∼50% lower ($n = 12$; **, $P < 0.01$) in comparison with $Ca_v\beta_{1b}$. The mRNA expression level for $Ca_v\beta_{4b}$ was not different from that of $Ca_v\beta_{1b}$. Error bars represent SEM. Bars (A–C), 25 μm; (D) 5 μm.

(Wittemann et al., 2000). In addition, the isolated N terminus of $Ca_v\beta_{4a}$ is capable of interacting with proteins of the vesicle release machinery (Vendel et al., 2006).

All $Ca_v\beta$ subunits are expressed in the brain. Their subcellular distribution within neurons reveals that they are localized to neuronal cell bodies and dendrites. In addition, $Ca_v\beta$ has been suggested to be localized to synaptic terminals (Herlitze and Mark, 2005). However, its precise function for determining synaptic transmission and, in particular, synaptic plasticity is unclear. Therefore, the goal of this study is to analyze the distribution of endogenously and exogenously expressed $Ca_v\beta$ subunits in hippocampal neurons and to correlate their distribution with their effects on synaptic transmission. Our results suggest that $Ca_v\beta_{2a}$ and $Ca_v\beta_{4b}$ subunits are targeted to presynaptic terminals, where they determine whether synapses facilitate or depress.

Results

Distribution of endogenous $Ca_v\beta$ subunits in hippocampal neurons

We first investigated whether hippocampal neurons in culture express endogenous $Ca_v\beta$ subunits, as would be predicted by the presence of the endogenous high voltage–activated Ca^{2+} channels (Reid et al., 1998; Wittemann et al., 2000). We produced a peptide-derived antibody, which recognizes all β-subunit family members (pan-β antibody). As indicated in Fig. 1 A, the antibody recognized specifically $Ca_v\beta$ subunits in hippocampal neurons, as demonstrated by antagonistic action of the epitope peptide (not depicted). Many, but not all, of the puncta colocalize with the synaptic markers synaptobrevin 2 (Fig. 1, A–C) and synapsin 1 (Fig. 1 D). The subunits are expressed throughout the neuron with high and uniform staining detected in the soma and proximal dendrites, with more clustered distribution in synaptic areas. We next analyzed whether we could detect $Ca_v\beta$ subunit–specific mRNAs in these neurons and whether we could see quantitative differences among the four different $Ca_v\beta$ mRNAs. As a positive control, we used 18S RNA. Real-time PCR revealed the highest mRNA levels for the $Ca_v\beta_3$ subunits and lower mRNA levels for $Ca_v\beta_{1,2,4}$ ($Ca_v\beta_1 \geq Ca_v\beta_4 \geq Ca_v\beta_2$; Fig. 1 E). The results indicate that all four $Ca_v\beta$ subunits are expressed in hippocampal neurons in culture, which localize to the soma and to synapses.

Distribution of exogenously expressed $Ca_v\beta$ subunits in hippocampal neurons

We next analyzed whether the exogenous expression of the $Ca_v\beta$ members resembles the endogenous distribution of the $Ca_v\beta$ subunits as determined in Fig. 1 and whether $Ca_v\beta$ subunits can target to synaptic sites when expressed alone in neurons (Fig. 2).

We found that the $Ca_v\beta_{1b}$ and $Ca_v\beta_3$ subunits reveal a more homogenous distribution, whereas the $Ca_v\beta_{2a}$ and $Ca_v\beta_{4b}$ subunits are highly clustered (Fig. 2, A–C). When cells expressing these exogenous subunits were immunostained with the synaptic marker synaptobrevin-II or synapsin-1, we found that $Ca_v\beta_{4b}$ subunits revealed a higher degree of colocalization with synaptic markers than $Ca_v\beta_{2a}$. Association of the $Ca_v\beta$ subunits with the $Ca_v\alpha_1$ subunits predicts that both proteins should be distributed in cytoplasmic as well as membrane regions, which we confirmed by Western blots from cytosolic and membrane fractions of whole rat brain using the pan-$Ca_v\beta$ antibody (Fig. 3, A and B). Exogenous expression of the $Ca_v\beta$ subunits revealed a similar distribution, with subtype-specific enrichment within either the cytoplasmic or the membrane fraction (Fig. 3 C). $Ca_v\beta_{2a}$ subunits are highly enriched in the membrane fraction, whereas $Ca_v\beta_{1b}$ was mostly concentrated in the cytoplasm (Fig. 3 C). $Ca_v\beta_3$ and $Ca_v\beta_4$ subunits were equally distributed in both fractions (Fig. 3 C).

Because Ca^{2+} channel $Ca_v\beta_{2a}$ and $Ca_v\beta_{4b}$ subunits reveal a mainly punctuate distribution within the neurons, we wanted to know whether we can detect $Ca_v\beta$ subunits in presynaptic terminals on vesicles or vesicular structures (Fig. 4). The high expression levels of the GFP-tagged subunits allowed us to study their localization by immunoelectron microscopy. As a negative control, we used the untagged GFP overexpressed in hippocampal neurons. As shown in Fig. 4, $Ca_v\beta_{2a}$ and $Ca_v\beta_{4b}$ subunits were detected on vesicular structures (Fig. 4, A and B) and close to presynaptic terminals (Fig. 4, C and D). We also observed that both $Ca_v\beta_{2a}$ and $Ca_v\beta_{4b}$ were attached to the plasma membrane (Fig. 4 D). In contrast, GFP was found only in the nucleus and outside of the nucleus but was not associated with vesicles or transported to the presynapse (unpublished data). The results suggest that both $Ca_v\beta_{2a}$ and $Ca_v\beta_{4b}$ subunits are transported to synaptic sites and to the plasma membrane, where they most likely associate with the $Ca_v\alpha_1$ subunits to form channel complexes.

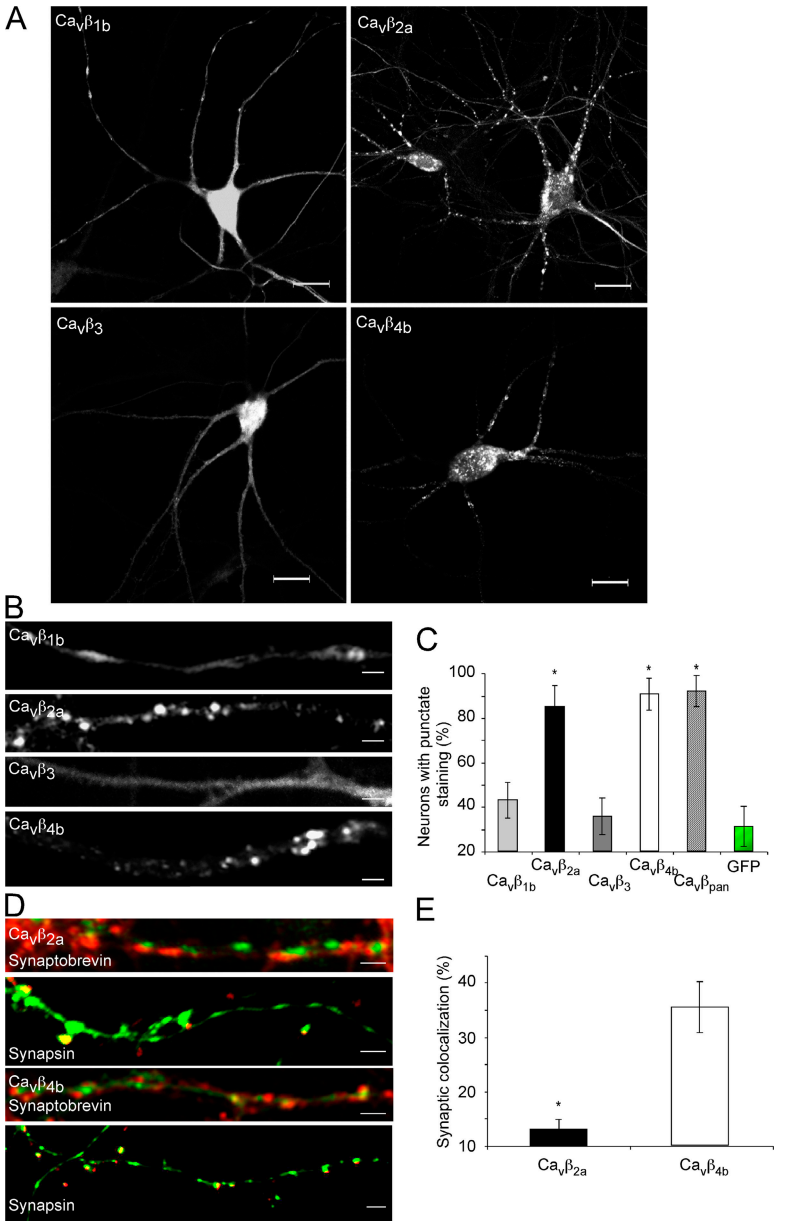

Figure 2. **Exogenously expressed $Ca_v\beta_{1-4}$ subunits distribute in different patterns in hippocampal neurons and colocalize to various degrees with presynaptic marker proteins.** (A) Fluorescence pattern of neurons from low density hippocampal cultures infected with the indicated GFP-tagged $Ca_v\beta$ subunit (i.e., $Ca_v\beta_{1-4}$) reveal either a punctate ($Ca_v\beta_{2a}$ and $Ca_v\beta_{4b}$) or a more diffuse, cytosolic staining ($Ca_v\beta_{1b}$ and $Ca_v\beta_3$). (B) Increased magnification of hippocampal neurites reveal that $Ca_v\beta_{2a}$ and $Ca_v\beta_{4b}$ are clustered, whereas $Ca_v\beta_{1b}$ and $Ca_v\beta_3$ are diffusely distributed. (C) The bar graph indicates that neurons overexpressing $Ca_v\beta_{2a}$ and $Ca_v\beta_{4b}$ mainly reveal punctate staining similar to the endogenous distribution of $Ca_v\beta$ subunits, whereas the majority of neurons infected with $Ca_v\beta_{1b}$ and $Ca_v\beta_3$ or GFP alone do not reveal punctate staining (n = 110–153 for each subunit; *, $P < 0.01$ compared with GFP). Quantification of the percentage of transfected neurons showing that punctate staining was performed by generating 11–13 randomly chosen fields within each group of neurons analyzed. In each field, the number of total infected neurons was counted, and the percentage of those showing punctate patterns was calculated. The percentages in each group were then averaged. n is equal to the total number of infected neurons counted. (D and E) $Ca_v\beta_{2a}$ and $Ca_v\beta_{4b}$ reveal differences in their percentages to colocalize with presynaptic marker proteins. (D) Cultured hippocampal neurons were infected with GFP-tagged $Ca_v\beta_{2a}$ and $Ca_v\beta_{4b}$ and costained with synaptobrevin-II or synapsin-I (red). Representative confocal images of hippocampal neurites reveal that the fluorescent puncta in $Ca_v\beta_{2a}$- and $Ca_v\beta_{4b}$ (green)-expressing neurons reveal a different colocalization percentage with the presynaptic marker (red). (E) Quantification of the GFP puncta containing either $Ca_v\beta_{2a}$ or $Ca_v\beta_{4b}$ that colocalize with synaptobrevin-II. The percentage of synaptic colocalization is given as the number of $Ca_v\beta$ GFP puncta, which colocalized with the number of synaptobrevin-II puncta relative to the amount of GFP puncta within the region of interest analyzed (n = 20–21; *, $P < 0.01$). Error bars represent SEM. Bars (A), 15 μm; (B and D) 2 μm.

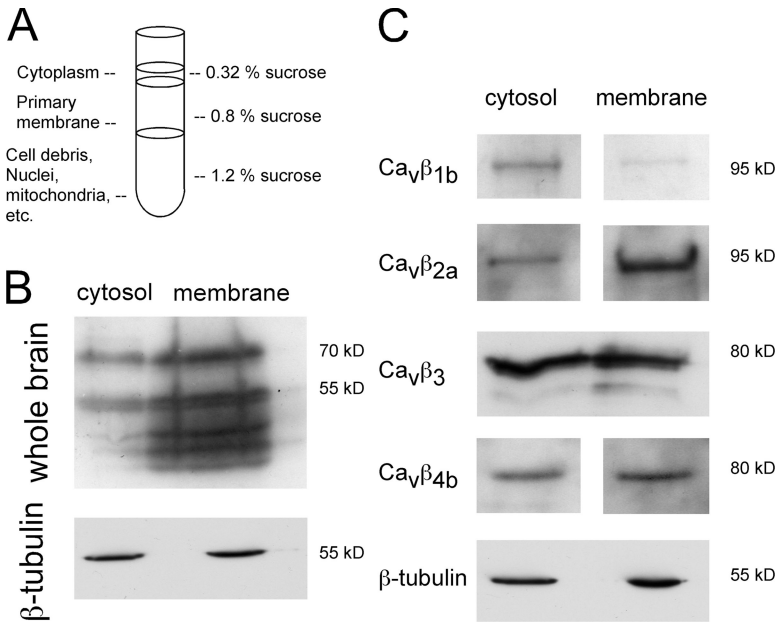

Figure 3. **$Ca_v\beta$ subunits are found in cytoplasmic and membrane fractions in hippocampal neurons.** (A and B) Rat whole brains (postnatal day 0–3) were homogenized and fractionated in a discontinuous sucrose gradient. Primary membrane and cytosolic fractions were taken for Western blot analysis. (B) When immunoblotted with the pan-β antibody, the endogenous $Ca_v\beta$ subunits were mainly located in the membrane fraction but also found in the cytosolic fraction. (C) Exogenously expressed $Ca_v\beta$ subunits revealed a subunit-specific distribution between the cytosolic and membrane fraction. 13–16 h after infection with $Ca_v\beta$ subunits, 14-d in vitro hippocampal neurons were harvested, and cell extracts were blotted with anti-GFP antibodies.

Effect of $Ca_v\beta$ subunits on Ca^{2+} channel currents in HEK293 cells and hippocampal neurons

$Ca_v\beta$ subunits determine the biophysical properties of the Ca^{2+} channel. When expressed with the P/Q-type channel in *Xenopus laevis* oocytes or HEK293 cells, $Ca_v\beta$ subunits determine the time course of inactivation in a subunit-specific manner. $Ca_v\beta_{1b}$- and $Ca_v\beta_3$-assembled channels inactivate rapidly, whereas $Ca_v\beta_{2a}$-assembled channels inactivate slowly (Stea et al., 1994). $Ca_v\beta_{4b}$-assembled channels inactivate with a time course that lies between $Ca_v\beta_{1b,3}$ and $Ca_v\beta_{2a}$. The gating properties of the presynaptic Ca^{2+} channels determine Ca^{2+} influx into the presynaptic terminal and, therefore, determine transmitter release and synaptic plasticity, such as facilitation and depression.

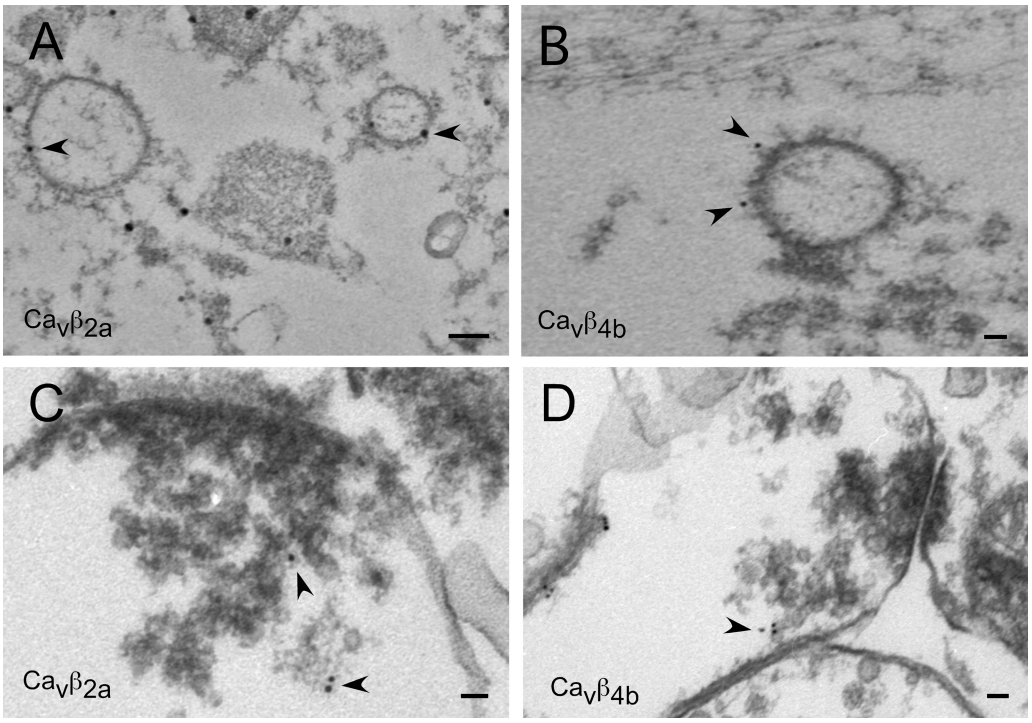

Figure 4. **Immunoelectron microscopy reveals that $Ca_v\beta_{2a}$ and $Ca_v\beta_{4b}$ subunits are associated with membranes and vesicular structures and are targeted to presynaptic terminals in hippocampal neurons.** (A and B) Immunoelectron microscopy pictures of 14-d in vitro autaptic neurons exogenously expressing GFP-tagged $Ca_v\beta_{2a}$ (A) or GFP-tagged $Ca_v\beta_{4b}$ (B) subunits. In neurons expressing $Ca_v\beta_{2a}$ and $Ca_v\beta_{4b}$ subunits, gold particles were found attached or close to vesicular structures (arrowheads). (C and D) In adult hippocampal slices, exogenously expressing GFP-tagged $Ca_v\beta_{2a}$ (C) and $Ca_v\beta_{4b}$ subunits (D) were found in presynaptic terminals close to synaptic vesicles and attached to the cell membranes (arrowheads). Bars, 50 nm.

We wanted to know how P/Q-type channels assembled with different $Ca_v\beta$ subunits open and closed during action potential (AP) waveforms, which we obtained from cultured hippocampal neurons. We expressed $Ca_v\alpha_1 2.1$ subunits together with the $Ca_v\alpha_2\delta$ and the various $Ca_v\beta$ subunits in HEK293 cells and applied 30 APs to analyze how many channels would be opened during AP trains. To determine the proportion of open channels, we used the following protocol. Based on the voltage dependence of the activation of P/Q-type channels, we applied a 10-ms depolarizing test pulse to a test potential in which ~100% of channels within the cells were open (Herlitze et al., 1996, 1997, 2001; Mark et al., 2000). This value is given by the amplitude of the tail current. We then compared the tail current elicited by the AP to the tail current elicited by the 10-ms depolarization to +100 mV. We were interested in three values. We wanted to know whether activation with the AP waveforms would reveal differences in the opening of the channels when assembled with different $Ca_v\beta$ subunits. The results indicated that the AP opens between 55 and 65% of the channels. No considerable differences were observed between channels assembled with the different $Ca_v\beta$ subunits (Fig. 5, A and B).

We next compared the ratio between the amount of channels opened by the first and the second AP (Fig. 5 A). By comparing this value, we gain information on differences on the influx of Ca^{2+} through Ca^{2+} channels into the presynaptic terminal, which may determine whether synapses facilitate or depress during paired pulses. No differences were detected between channels assembled with different $Ca_v\beta$ subunits. We next analyzed whether a 20-Hz train of 30 APs leads to a decrease in channel opening, as would be expected from the inactivation of Ca^{2+} channels during long, constant depolarizations (Stea et al., 1994; Herlitze et al., 1997). When comparing the proportion of channels opened by the first AP relative to the amount of channels opened by the 30th AP, we found that currents mediated by

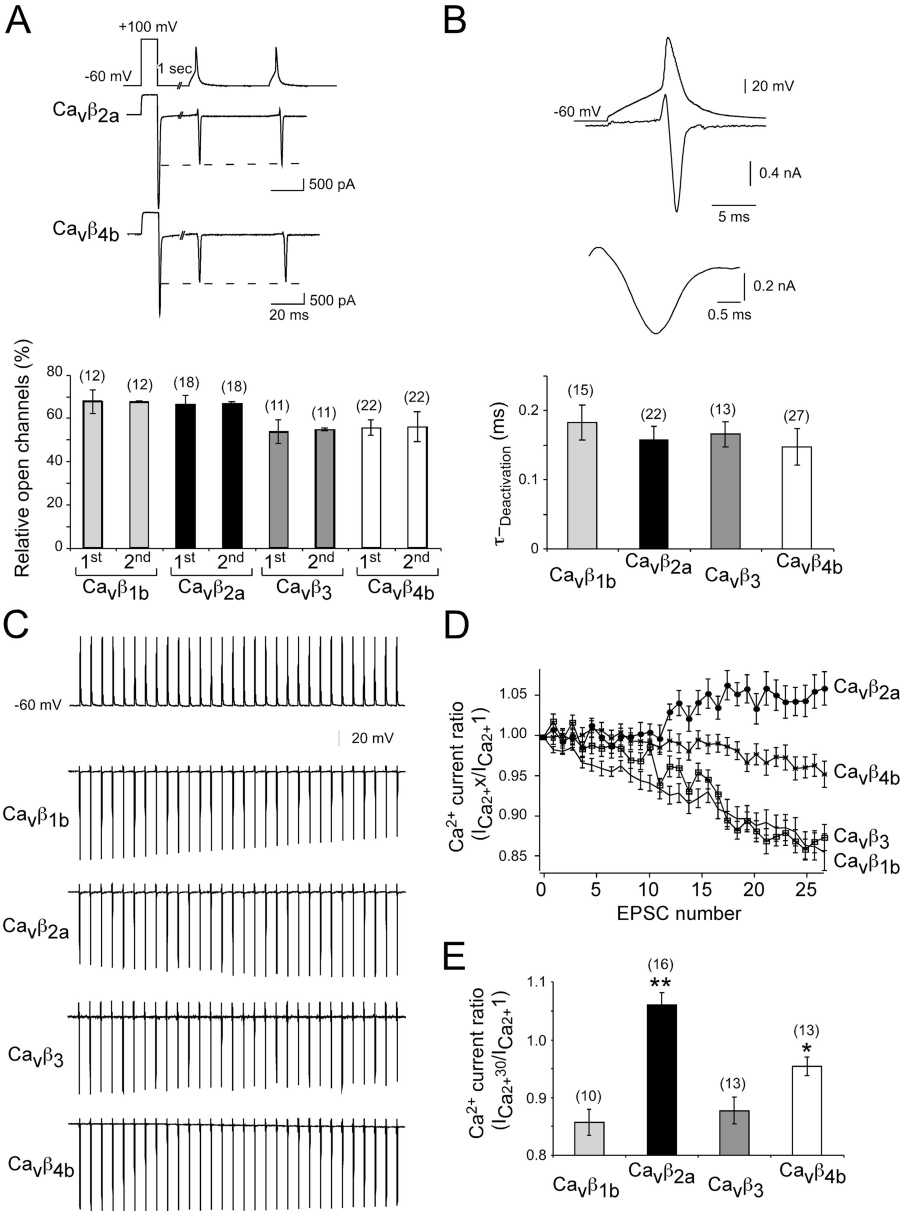

Figure 5. **Hippocampal AP waveform protocols detect differences in the amount of open P/Q-type channels assembled with the different $Ca_v\beta$ subunits during long 20-Hz stimulations but not for paired pulses.** (A) HEK293 cells expressing $Ca_v\alpha_1 2.1$, $Ca_v\alpha_2\delta$, and one of the four $Ca_v\beta_{1b}$, $Ca_v\beta_{2a}$, $Ca_v\beta_3$, and $Ca_v\beta_{4b}$ subunits were held at −60 mV, and Ca^{2+} currents were elicited by a 20-Hz AP train 1 s after a prepulse to 100 mV for 10 ms. This prepulse was given to open ~100% of the Ca^{2+} channels expressed in the cell (top). The tail current elicited by the prepulse was used to relate the tail current elicited by the AP to gain an understanding about the percentage of channels opened by the AP. The example whole cell currents (top) and the bar graph (bottom) indicate that approximately the same amount of channels were opened by the first AP and the second AP for the $Ca_v\beta_{1-4}$-assembled P/Q-type channels analyzed. (B) Increased time resolution of the underlying current elicited by the AP. The deactivation time of the tail currents can be fitted with a single exponential. Only currents were included and analyzed in the experiments described in A–E, which reveal fast deactivation kinetics and no change in the deactivation kinetics between the first and the last tail current elicited. (C) Examples of P/Q-type channel currents assembled with $Ca_v\beta_{1-4}$ subunits during a 20-Hz 30-pulse AP waveform train. (D) Relative ICa^{2+} ratio for the P/Q-type channel currents assembled with $Ca_v\beta_{1-4}$ subunits. The tail current amplitudes were related to the tail current elicited by the first AP. (E) Comparison of the relative amplitude of the tail currents elicited by the first and 30th AP during the 20-Hz AP train reveals that currents through P/Q-type channels assembled with $Ca_v\beta_{1b}$ and $Ca_v\beta_3$ subunits are relatively smaller than currents through P/Q-type channels assembled with $Ca_v\beta_{2a}$ and $Ca_v\beta_{4b}$. Error bars represent SEM. *, $P < 0.05$; **, $P < 0.01$.

$Ca_v\beta_{1b}$- and $Ca_v\beta_3$-assembled channels are reduced by 10–15% (Fig. 5, D and E). In contrast, currents mediated by $Ca_v\beta_{4b}$-assembled channels are reduced by 2% (Fig. 5, D and E), and currents mediated by $Ca_v\beta_{2a}$-assembled channels increased by 5% (Fig. 5, D and E). Thus, P/Q-type channels assembled with different β subunits reveal substantial differences in the amount of channel opening during long AP trains.

It has been shown that the biophysical properties of P/Q-type channels depends on the cellular environment in which the pore-forming $Ca_v\alpha_1$ subunit is expressed (Tottene et al., 2002). We found that the maximal current elicited by a 500-ms-long voltage ramp is shifted to more negative potentials (around 20 mV) in neurons expressing non–L-type channels in comparison with HEK293 cells expressing P/Q-type channels encoded by the $Ca_v\alpha_1$2.1, $Ca_v\alpha_2\delta$, and $Ca_v\beta$ subunits (Fig. 6 A). Therefore, $Ca_v\beta$ subunit–mediated effects on presynaptic Ca^{2+} channel (non–L type) inactivation may be shielded in neurons by, for example, neuronal-specific channel-interacting proteins. To show that the $Ca_v\beta$ subunits (i.e., $Ca_v\beta_{2a}$ and $Ca_v\beta_{4b}$) also change the biophysical properties of non–L-type channels in hippocampal neurons, we analyzed the Ca^{2+} channel inactivation of somatic neuronal non–L-type channels. As shown in Fig. 6 B, the exogenous expression of $Ca_v\beta_{2a}$ and $Ca_v\beta_{4b}$ subunits reduce non–L-type channel inactivation in a subunit-specific manner. $Ca_v\beta_{2a}$ subunit expression leads to an increase in the non–L-type current during a 100-ms test pulse from −60 to 0 mV, whereas neuronal non–L-type currents in the presence of $Ca_v\beta_{4b}$ subunits do not change in size (Fig. 6 B).

Effects of $Ca_v\beta$ subunits on synaptic transmission

Our results on the recombinant P/Q-type channels and endogenous neuronal Ca^{2+} channels suggest that Ca^{2+} influx into the presynaptic terminal should be altered during long 20-Hz AP trains but not for paired-pulse responses. We analyzed the effect of the $Ca_v\beta$ subunits on paired-pulse facilitation (PPF) by comparing the first and second excitatory postsynaptic current (EPSC; defined as the paired-pulse ratio [PPR]) and analyzed the effect on synaptic depression by comparing the first and last EPSCs (averaged 27–30 EPSCs) within a 20-Hz stimulation protocol when 30 pulses were elicited in 4 mM of extracellular Ca^{2+} (Fig. 7, A and C). Because we did not observe effects on synaptic transmission when $Ca_v\beta_{1b}$ and $Ca_v\beta_3$ subunits were expressed in our initial studies (unpublished data), we only analyzed $Ca_v\beta_{4b}$ and $Ca_v\beta_{2a}$ subunit effects on synaptic transmission in the following experiments. According to our results regarding the effects of $Ca_v\beta$ subunits on the inactivation properties of Ca_v2 channels, we found that $Ca_v\beta_{2a}$ subunits did not change the PPR as expected from the aforementioned biophysical analysis. However, $Ca_v\beta_{4b}$ subunits increased the PPR, leading to facilitation (Fig. 7, A and C).

We next analyzed whether the $Ca_v\beta_{4b}$ and $Ca_v\beta_{2a}$ subunits influence synaptic transmission during longer AP trains. The biophysical analysis predicts that in the presence of $Ca_v\beta_{4b}$ and $Ca_v\beta_{2a}$ subunits, Ca^{2+} influx into the presynaptic terminal should be increased as a result of the noninactivating properties of the presynaptic Ca^{2+} channels in comparison with $Ca_v\beta_{1b}$ and $Ca_v\beta_3$ subunits. The increased Ca^{2+} influx may cause more vesicle depletion (depression) and may influence asynchronous transmitter release, which has been shown to be proportional to the residual $[Ca^{2+}]_i$ (Atluri and Regehr, 1998). Analysis of the synaptic responses during 30 20-Hz AP trains revealed that $Ca_v\beta_{4b}$- and $Ca_v\beta_{2a}$-expressing neurons show larger depression in comparison with wild-type neurons (Fig. 7, A–C) Note that the amount of depression is related to the largest EPSC compared with the minimal EPSC at the end of the stimulus train. The largest EPSC in noninfected neurons and $Ca_v\beta_{4b}$-expressing neurons is the EPSC elicited by the second pulse. Therefore, depression is significantly larger for $Ca_v\beta_{2a}$ (0.34 ± 0.01; $n = 14$) as well as for $Ca_v\beta_{4b}$ (0.49 ± 0.03; $n = 15$) in comparison with noninfected neurons (0.7 ± 0.01; $n = 15$). To determine whether

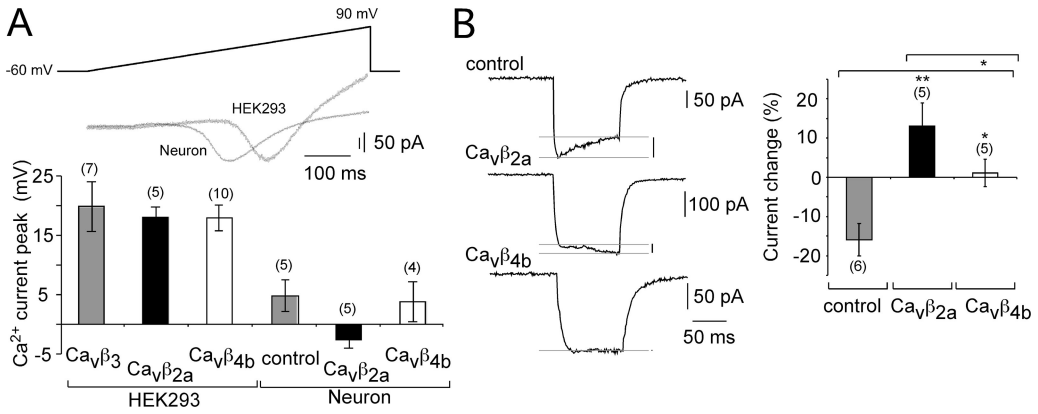

Figure 6. **$Ca_v\beta$ subunits expressed in hippocampal neurons change the biophysical properties of the endogenous non–L-type channels.** (A) The activation of non–L-type channels in hippocampal neurons is shifted to more negative potentials when compared with P/Q-type channels exogenously expressed in HEK293 cells. (top) Example current traces (IV curve) of non–L-type currents from hippocampal neurons in comparison with currents through P/Q-type channels ($Ca_v\alpha_1$2.1, $Ca_v\alpha_2\delta$, and $Ca_v\beta_{4b}$) expressed in HEK293 cells elicited by 500-ms voltage ramps from −60 to 90 mV. (bottom) Diagram of the voltage at which the peak current appears during the voltage ramp for P/Q-type channels expressed in HEK293 cells and non–L-type currents from hippocampal neurons in the presence or absence of $Ca_v\beta_{2a}$ and $Ca_v\beta_{4b}$ subunits. (B) The inactivation properties of non–L-type channels in hippocampal neurons are changed in the presence of $Ca_v\beta_{2a}$ and $Ca_v\beta_{4b}$ subunits. (left) Example traces of non–L-type currents elicited by a voltage pulse from −60 to 0 mV reveals that in the presence of $Ca_v\beta_{2a}$ and $Ca_v\beta_{4b}$ subunits, inactivation is slowed. (right) Diagram of the current change (percentage) within the 100-ms current trace. The current at the beginning of the test pulse (10 ms) is compared with the current at the end of the test pulse (95 ms). Error bars represent SEM. *, $P < 0.05$; **, $P < 0.01$.

$Ca_v\beta_{4b}$- and $Ca_v\beta_{2a}$-expressing neurons reveal more vesicle depletion during AP trains, we compared the readily releasable pool size before and after 20-Hz train stimulations. As shown in Fig. 7 (E and F), the pool size is substantially reduced in $Ca_v\beta_{2a}$-expressing neurons (12 ± 3.5%) and is slightly reduced in $Ca_v\beta_{4b}$-expressing neurons (9 ± 2.7%) in comparison with control neurons (3 ± 2.2%). However, the $Ca_v\beta_{4b}$ effects were not substantial. To further verify that $Ca_v\beta_{4b}$- and $Ca_v\beta_{2a}$-expressing neurons may increase the Ca^{2+} influx into the presynaptic terminal, we analyzed the asynchronous release. We found that onset of the asynchronous release was much faster and the amount of asynchronous relative to the phasic release at the beginning of the AP train was increased in $Ca_v\beta_{4b}$- and $Ca_v\beta_{2a}$-expressing neurons in comparison with control neurons (Fig. 7 G). Although the total amount of phasic and asynchronous release (Fig. 7 H) as well as the mean EPSC amplitude (Fig. 7 D) were slightly increased in $Ca_v\beta_{4b}$-expressing neurons in comparison with control and $Ca_v\beta_{2a}$-expressing neurons, the differences were not substantial.

These aforementioned results support the idea that during AP trains, the Ca^{2+} influx into the presynaptic terminal is larger in the presence of $Ca_v\beta_{4b}$ and $Ca_v\beta_{2a}$ subunits. A larger Ca^{2+} influx into the presynaptic terminal during AP trains in $Ca_v\beta_{4b}$ and $Ca_v\beta_{2a}$ subunit–expressing neurons should also result in faster

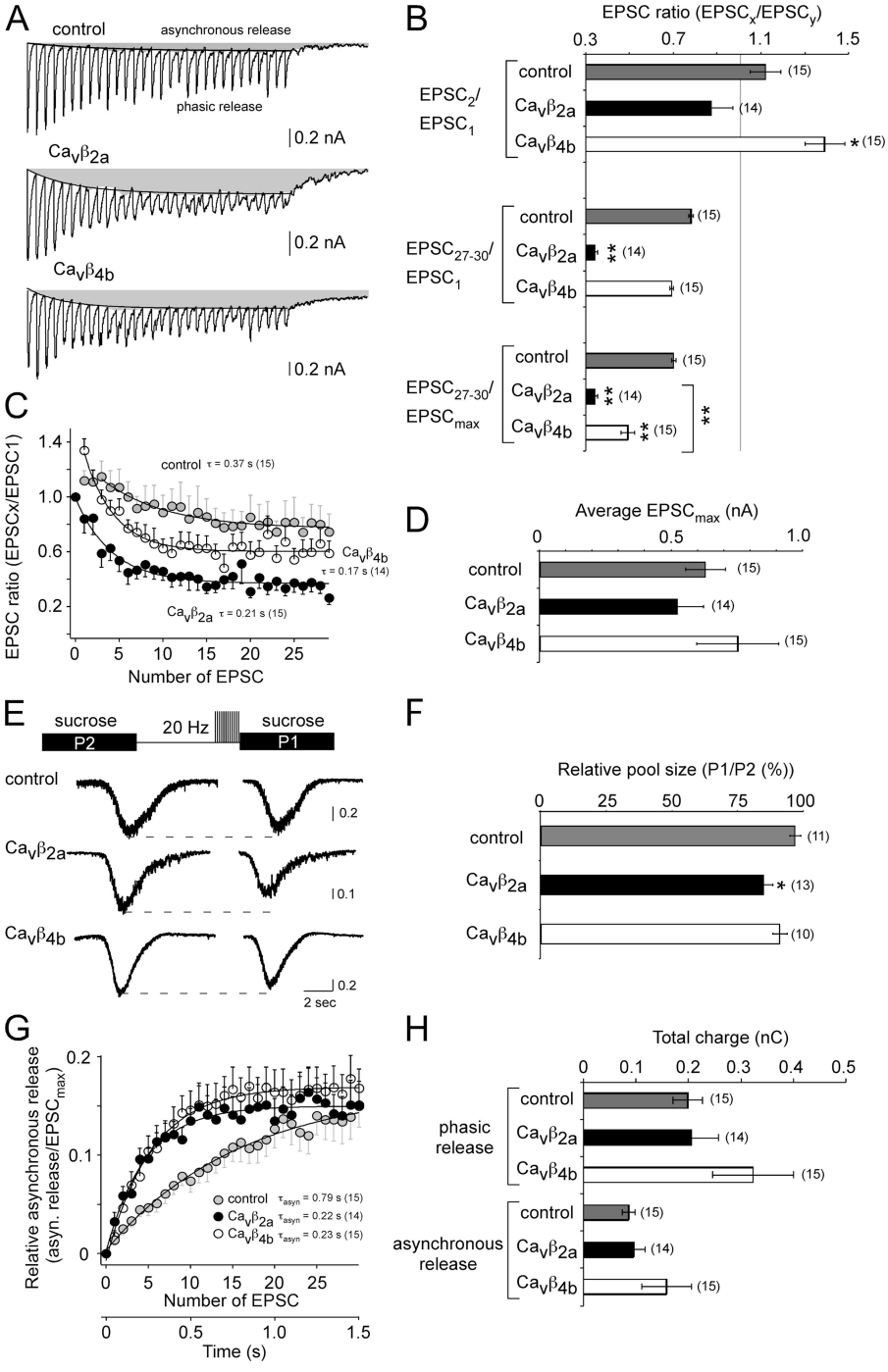

Figure 7. **$Ca_v\beta$ subunit–specific determination of facilitation and depression in autaptic hippocampal neurons.** (A and B) EPSC recordings of autaptic hippocampal neurons exogenously expressing $Ca_v\beta_{2a}$ and $Ca_v\beta_{4b}$ subunits in 4 mM Ca^{2+}. (A) Representative autaptic EPSC traces from noninfected and $Ca_v\beta_{2a}$ and $Ca_v\beta_{4b}$ subunit–infected neurons reveal that in the presence of $Ca_v\beta_{2a}$ and $Ca_v\beta_{4b}$ subunits, synaptic depression is increased during long 20-Hz stimulations. Gray areas represent the asynchronous release. (B) Bar graph of the quantified EPSC ratios of $Ca_v\beta_{2a}$ and $Ca_v\beta_{4b}$ subunit–infected and noninfected neurons. The EPSC amplitudes of the first and second EPSC (top), the first and the mean from the 27–30th EPSC (middle), and the largest EPSC during a train and the mean from the 27–30th EPSC (bottom). (C) Relative EPSCs for $Ca_v\beta_{2a}$- and $Ca_v\beta_{4b}$-infected and noninfected neurons. The EPSC amplitudes during the 20-Hz pulse train were related to the EPSC elicited by the first pulse. The decline in EPSC amplitude could be fitted with a single exponential starting from the largest EPSC within the pulse train. (D) Bar graph of the mean maximal EPSC amplitude of $Ca_v\beta_{2a}$ and $Ca_v\beta_{4b}$ subunit–infected and noninfected neurons during a 20-Hz pulse train. (E and F) Comparison of the RRP before and after 30 2-ms-long pulses to 10 mV (20-Hz stimulation). (E) Example traces of sucrose responses before (P2) and after the 20-Hz stimulation (P1). (F) Relative pool size for $Ca_v\beta_{2a}$- and $Ca_v\beta_{4b}$-infected and noninfected neurons. The relative pool size was determined by the ratio between the sucrose response after the 20-Hz stimulation (P1) and the sucrose response before the stimulation (P2). (G) Time course of asynchronous release during a 20-Hz pulse train. The charge of the largest EPSC ($EPSC_{max}$) within the 20-Hz train was compared with the charge of the asynchronous release for each EPSC. (H) Bar graph of the quantified total charge during a 20-Hz stimulation protocol for the phasic release and asynchronous release for $Ca_v\beta_{2a}$- and $Ca_v\beta_{4b}$-infected and noninfected neurons. The mean values of the time course of depression (C) and the asynchronous release (G) were fitted with a single exponential, and the time constants for each fit and the number of experiments (given in parentheses) are given in the diagrams. Error bars represent SEM. * P, < 0.05; **, $P < 0.01$.

vesicle recycling (Stevens and Wesseling, 1998). To test this hypothesis, we repeated the experiments described in Stevens and Wesseling (1998). We first analyzed the recovery of the readily releasable vesicle pool (RRP) after RRP depletion without 20-Hz stimulation trains applied during depletion. No differences were found for the recovery of the RRP regardless of whether $Ca_v\beta_{4b}$ or $Ca_v\beta_{2a}$ subunits were expressed in the neurons (Fig. 8, A and B). Also, recovery of the EPSC after RRP depletion was not different between neurons expressing or not expressing $Ca_v\beta_{4b}$ and $Ca_v\beta_{2a}$ subunits (Fig. 8, C and D), suggesting that exogenously expressed $Ca_v\beta_{4b}$ and $Ca_v\beta_{2a}$ subunits most likely do not interfere with the vesicle recycling. We next analyzed the RRP recovery after 20-Hz stimulation trains were applied during the initial sucrose application (Fig. 8 E). We confirmed the observation described by Stevens and Wesseling (1998) that the RRP recovery for all neurons analyzed (regardless of whether $Ca_v\beta$ subunits were expressed or not) was accelerated by the 20-Hz stimulus train (Fig. 8, E and F). Interestingly, RRP recovery was faster in $Ca_v\beta_{4b}$ and $Ca_v\beta_{2a}$ subunit–expressing neurons in comparison with control neurons (τ_{rec} without 20-Hz train stimulation: control = 11.4 s, $Ca_v\beta_{2a}$ = 9.1 s, and $Ca_v\beta_{4b}$ = 12.6 s; τ_{rec} after 20-Hz train stimulation: control = 4.1 s, $Ca_v\beta_{2a}$ = 1.8 s, and $Ca_v\beta_{4b}$ = 1.6 s), suggesting again that Ca^{2+} influx into the presynaptic terminal is increased during 20-Hz stimulation trains in $Ca_v\beta_{4b}$ and $Ca_v\beta_{2a}$ subunit–expressing neurons.

Although the exogenous expression of $Ca_v\beta$ subunits determines the synaptic responses during long AP trains according to the biophysical properties of the assembled presynaptic Ca^{2+} channels, the induced facilitation by $Ca_v\beta_{4b}$ during paired pulses cannot be explained by the biophysical properties of presynaptic Ca^{2+} channel assembled with the $Ca_v\beta_{4b}$ subunit. However, this may suggest that in the presence of $Ca_v\beta_{4b}$ subunit,

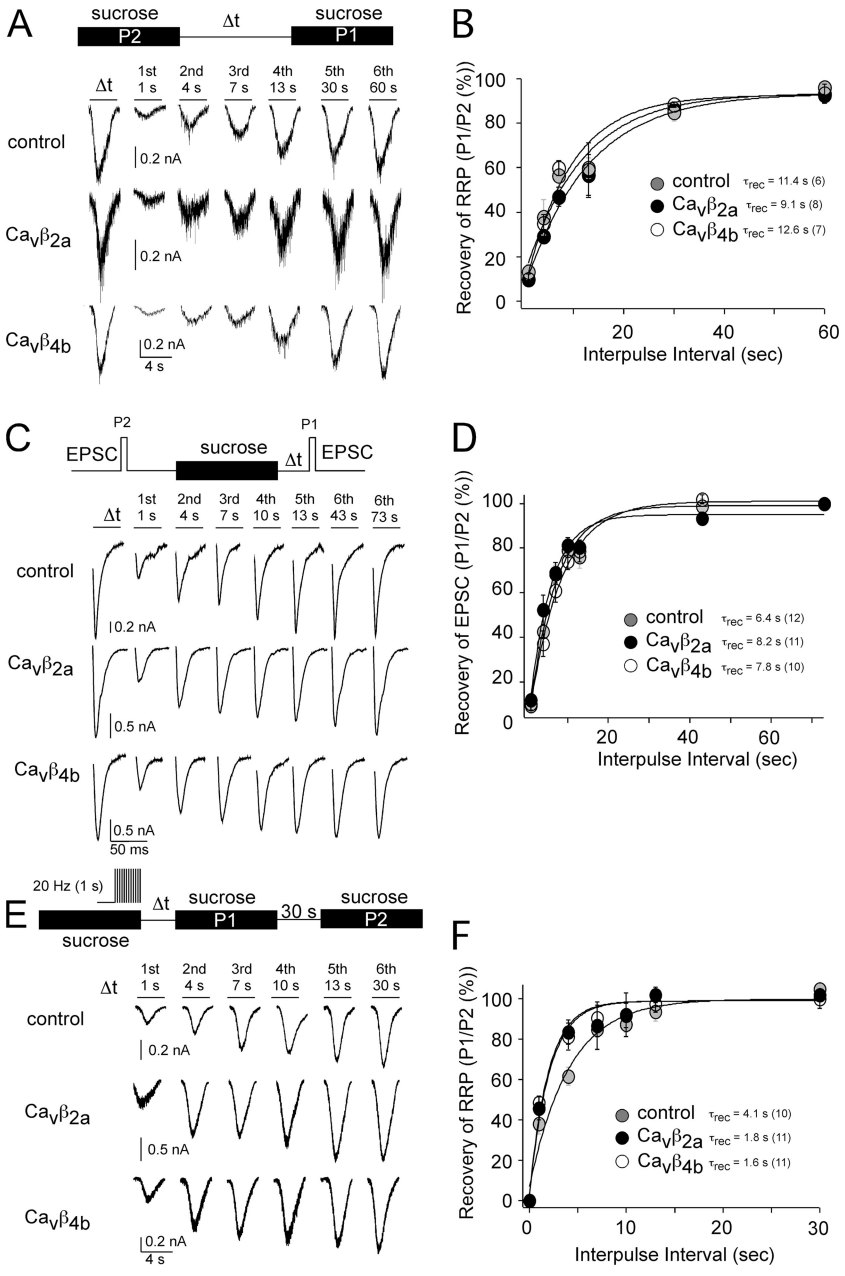

Figure 8. **$Ca_v\beta_{2a}$ and $Ca_v\beta_{4b}$ subunits expressed in hippocampal neurons accelerate the recovery of the readily releasable pool when trains of APs have been evoked previously.** To evaluate whether $Ca_v\beta_{2a}$ and $Ca_v\beta_{4b}$ subunits affect vesicle recycling, we analyzed the recovery of the RRP and the EPSC after RRP depletion. The RRP was measured by applying hypertonic solution (500 mM sucrose) for 4 s. (A) Example traces of the time-dependent RRP recovery. (B) Time course of the recovery of the RRP. There were no substantial differences in the time course of RRP recovery between $Ca_v\beta_{2a}$- and $Ca_v\beta_{4b}$-expressing and nonexpressing neurons. (C) Example traces of the EPSC recovery after RRP depletion. (D) Time course of the recovery of the EPSC after RRP depletion. EPSCs were elicited by a 2-ms test pulse to 10 mV. (E) Example traces of the time-dependent RRP recovery when 20 stimulus trains have been evoked for 1 s at the end of the first sucrose application. (F) Time course of the recovery of the RRP reveals that in the presence of $Ca_v\beta_{2a}$ and $Ca_v\beta_{4b}$, the RRP recovery is faster. The relative recovery of the RRP and the EPSC was calculated by comparing the sucrose or EPSC response after the initial sucrose response to the initial (first) response. For RRP recovery in E and F, the sucrose response after the first depletion (P1) was compared with the sucrose response 30 s after the second sucrose response (P2). The interpulse intervals are given in A, C, and E. The mean values of the recovery of the RRPs and EPSCs shown in B, D, and F were fitted with a single exponential, and the time constant for each fit are given in the diagram. The numbers of experiments are given in parentheses. Error bars represent SEM.

the Ca^{2+} dependence of the vesicle release is altered, which may result in a reduced release probability (Thomson, 2000). Therefore, we compared the release probability of noninfected and $Ca_v\beta_{2a}$- as well as $Ca_v\beta_{4b}$-expressing neurons. The release probability can be examined by comparing the RRP with the number of vesicles elicited by a single AP. The RRP size is determined by application of a hypertonic sucrose solution (Rosenmund and Stevens, 1996). As shown in Fig. 9, we found that the release probability in the presence of $Ca_v\beta_{4b}$ was reduced in comparison with noninfected and $Ca_v\beta_{2a}$-expressing neurons. No differences in the mean RRP and EPSC size were detected between the neurons expressing different $Ca_v\beta$ subunits, probably because only a small number of cells were analyzed.

The relationship between the Ca^{2+} influx into the presynaptic terminal and the vesicle release is approximately given by the following equation: vesicle release $\propto [Ca^{2+}]^{\text{Hill coefficient}}$, where the Hill coefficient is defined as the Ca^{2+} cooperativity. The Ca^{2+} cooperativity in many synapses is high (three to four), indicating that a small change in Ca^{2+} influx can result in drastic changes in transmitter release. Thus, in our experiments, the Hill coefficient gives an indirect measure of the Ca^{2+} influx through presynaptic Ca^{2+} channels relative to the transmitter release. This means that a change in the number, localization, or organization of the presynaptic Ca^{2+} channels most likely results in a change in Ca^{2+} dependence of the transmitter release. Interestingly, in the presence of the $Ca_v\beta_{4b}$ subunits, the Ca^{2+}-dependent transmitter release dose-response curve became more shallow, with a small change in the half maximal $[Ca^{2+}]$ concentration (EC_{50}) when compared with wild-type neurons or neurons exogenously expressing $Ca_v\beta_{2a}$ subunits (Fig. 9). Because the $Ca_v\beta_{4b}$ subunit particularly changed the cooperativity of the transmitter release, this result may suggest that $Ca_v\beta_{4b}$ is involved in organization of the Ca^{2+} channel domains necessary for efficient vesicle release. For example, $Ca_v\beta_{4b}$-assembled channels may be further apart from the release machinery. If this is the case, synaptic transmission in $Ca_v\beta_{4b}$-expressing neurons should be more sensitive to the slow Ca^{2+} buffer EGTA. Indeed, we found that when 10 mM EGTA was applied intracellularly or 50 μM EGTA-AM was applied extracellularly, the EPSC amplitude was substantially more reduced in $Ca_v\beta_{4b}$-expressing neurons to 60 and 93%, whereas in $Ca_v\beta_{2a}$-expressing neurons and control neurons, the EPSC amplitude was reduced only by 50 and 87–89% (Fig. 9, E and F).

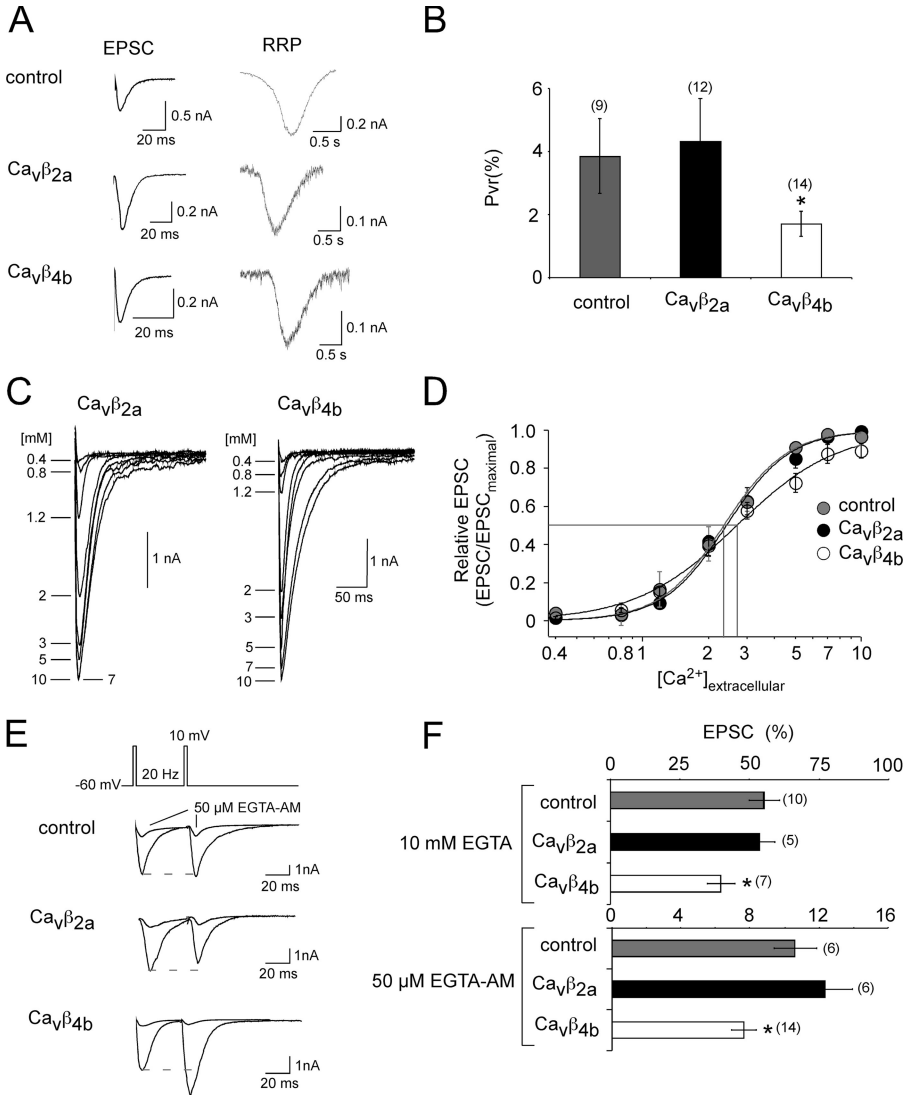

Figure 9. **$Ca_v\beta_{4b}$ subunits expressed in hippocampal neurons reduce the synaptic release probability, change the Ca^{2+}-dependent transmitter release, and are more sensitive to EGTA.** (A, left) Representative EPSC traces evoked by 2-ms depolarizing pulses from −60 to 10 mV are shown for noninfected and $Ca_v\beta_{2a}$- and $Ca_v\beta_{4b}$-infected neurons. (right) Representative traces of the hypertonically mediated release of quanta from the same neuron shown on the left upon the application of 500 mM sucrose for 4 s. (B) Probability of synaptic vesicle release was evaluated by calculating the ratio of release evoked by the AP to that evoked by hypertonic sucrose. In autaptic neurons infected with $Ca_v\beta_{4b}$, the vesicular release probability is significantly reduced compared with noninfected or $Ca_v\beta_{2a}$ subunit–infected neurons. (C) Representative EPSC traces elicited by the application of increasing extracellular Ca^{2+} concentrations of autaptic hippocampal neurons expressing $Ca_v\beta_{4b}$ subunits. (D) Dose-response curve of the EPSC amplitude by increasing extracellular Ca^{2+} concentrations. The Ca^{2+}-dependent EPSC responses of noninfected, $Ca_v\beta_{4b}$-, or $Ca_v\beta_{2a}$-infected neurons were free fitted according to the Hill equation ($EPSC = EPSC_{maximal}/(1 + (EC_{50}/[Ca^{2+}]_o)^{\text{Hill coefficient}})$). The EPSCs were then normalized to the maximal EPSC given by each fit. The mean normalized EPSCs for the given Ca^{2+} concentrations are shown. The curves again were fitted according to the Hill equation. The Hill coefficients are 2.7 ± 0.4 for control and $Ca_v\beta_{2a}$-infected neurons and 1.9 ± 0.4 for $Ca_v\beta_{4b}$-infected neurons. (E) Representative EPSC traces before and after a 50-μM EGTA-AM application evoked by two 2-ms depolarizing pulses from −60 to 10 mV within 50 ms are shown for noninfected and $Ca_v\beta_{2a}$- and $Ca_v\beta_{4b}$-infected neurons. (F) Bar graph of the remaining EPSC amplitude after 10 mM EGTA was applied intracellularly for 20 min (top) and after 50 μM EGTA-AM was applied extracellularly for 15 min (bottom). Error bars represent SEM. *, $P < 0.05$.

Discussion

In this study, we investigated the targeting and function of $Ca_v\beta$ subunits in hippocampal neurons. We found that $Ca_v\beta_{2a}$ and $Ca_v\beta_{4b}$ are sufficiently targeted to synaptic sites, where they influence synaptic transmission during long AP trains according to the biophysical properties that these subunits induce in the presynaptic Ca^{2+} channel. During paired pulses, $Ca_v\beta_{4b}$ subunits also altered the Ca^{2+} dependence of transmitter release. The physiological consequences and implications of the findings are discussed below.

Targeting of $Ca_v\beta$ subunits to the plasma membrane and synaptic terminals

We show that $Ca_v\beta_{2a}$ and $Ca_v\beta_{4b}$ are targeted to synaptic sites and colocalize with synaptic markers. All $Ca_v\beta$ subunits (exogenously and endogenously expressed) are found to various degrees in cytoplasmic and membrane fractions, as suggested by an overexpression study of $Ca_v\beta$ subunits in HEK293 cells (Chien et al., 1998). In particular, $Ca_v\beta_{2a}$ subunits are associated with the membrane fraction, as predicted from their N-terminal located palmitoylation site (Dolphin, 2003; Herlitze et al., 2003). This is in agreement with previous studies performed in HEK293 cells in which palmitoylated $Ca_v\beta_{2a}$ subunits reach the plasma membrane independently of the $Ca_v\alpha_1$ subunit (Chien et al., 1998; Bogdanov et al., 2000). $Ca_v\beta_{2a}$ subunits could also be found on vesicular structures, supporting the view that they most likely are associated with $Ca_v\alpha_1$ subunits, where they are transported as preassembled channel complexes to synaptic sites (Ahmari et al., 2000; Shapira et al., 2003). Our studies for $Ca_v\beta_{1b}$ and $Ca_v\beta_3$ reveal that these subunits, when expressed alone, distribute more homogenously in neurons and do not substantially influence the synaptic parameters analyzed. The reason for this could be that $Ca_v\beta_{1b}$ and $Ca_v\beta_3$ are not sufficiently transported to the presynaptic terminals as suggested by Maximov and Bezprozvanny (2002). On the other hand, because $Ca_v\beta_3$ is the main mRNA detected in hippocampal neurons, most synaptic Ca^{2+} channels could be assembled with $Ca_v\beta_3$ subunits. Therefore, the biophysical properties of the presynaptic Ca^{2+} channels would not be affected by either $Ca_v\beta_{1b}$ and $Ca_v\beta_3$, because the biophysical differences of channels assembled with these subunits are small.

$Ca_v\beta$ subunits may determine synaptic plasticity during longer AP trains as a result of the effects on the inactivation properties of the presynaptic Ca^{2+} channel complexes

$Ca_v\beta$ in particular determines the time course of inactivation of high voltage–activated Ca^{2+} channels. How P/Q-type channels assembled with different $Ca_v\beta$ subunits behave when AP waveforms derived from hippocampal neurons are used as command potentials has not been studied before. Interestingly, we did not detect substantial differences in the opening of the channels for the first two APs, which would determine the Ca^{2+} influx into the presynaptic terminal during paired pulses underlying short-term synaptic plasticity, but found that $Ca_v\beta_{1b}$- and $Ca_v\beta_3$-assembled channels exhibited substantial differences in the proportion of channels open after 30 APs or longer trains when compared with the $Ca_v\beta_{2a}$- and $Ca_v\beta_{4b}$-assembled channels (20 Hz; Fig. 5 D). We have to point out that the determination of the biophysical properties of the P/Q-type channel in HEK293 cells cannot directly be compared with the effects these subunits have on the native presynaptic Ca^{2+} channels. For example, Tottene et al. (2002) showed that the maximal current amplitude (when the peak current was analyzed with voltage step protocols) of the pore-forming human $Ca_v\alpha_1 2.1$ subunit expressed in neurons from $Ca_v\alpha_1 2.1$ knockout mice was shifted by −20 mV when compared with the same channel subunit coexpressed with $Ca_v\alpha_{2b}\delta$ and $Ca_v\beta_{2e}$ in HEK293 cells. A similar shift in the maximal current amplitude was seen in our experiments when we compared the voltage ramps of rat $Ca_v\alpha_1 2.1$-, $Ca_v\alpha_2\delta$-, and $Ca_v\beta_{2a,4b}$-assembled channels in HEK293 cells with the non–L-type currents elicited by voltage ramps in noninfected or $Ca_v\beta$ subunit–infected neurons. This indicates that non–L-type currents in neurons differ in their biophysical properties probably because of cell type–specific interacting proteins and variations as well as combinations of splice variants contributing to the non–L-type current. The differences in channel opening and, therefore, Ca^{2+} influx correlate well with the observed effects $Ca_v\beta$ subunits have on synaptic depression, asynchronous release, and activity-dependent RRP recovery.

Synaptic depression can be achieved via various cellular mechanisms. Therefore, an increase in Ca^{2+} influx leading to faster vesicle depletion is only one possibility (Zucker and Regehr, 2002). Synaptic depression can also be independent of vesicle depletion. For example, a decrease in presynaptic Ca^{2+} influx into the calyx of Held is the major cause of synaptic depression at this synapse type (Xu and Wu, 2005). In addition, a reduction in the AP amplitude during high repetitive firing (>20 Hz) has been correlated with a reduction in the transmitter release (Brody and Yue, 2000). Because we did not observe any change in the AP amplitude when we elicited and measured 20-Hz AP trains in the presence or absence of $Ca_v\beta_{2a}$ and $Ca_v\beta_{4b}$ subunits, a decline in AP amplitude is most likely not involved in the depression effects observed (Fig. S1, available at http://www.jcb.org/cgi/content/full/jcb.200702072/DC1). Because our synaptic terminals are too small to directly record the Ca^{2+} influx, we cannot exclude the possibility that the presynaptic Ca^{2+} influx into the terminal is reduced. However, the decrease in channel inactivation, particularly for $Ca_v\beta_{2a}$ subunit–assembled channels, correlated with the faster RRP recovery and faster onset of asynchronous release does not agree with this mechanism but rather suggests a larger Ca^{2+} influx into the presynaptic terminal.

$Ca_v\beta_{4b}$ subunits change the cooperativity of transmitter release

Exogenous expression of $Ca_v\beta_{4b}$ subunits induced PPF. PPF occurs at low release probability synapses during high frequency stimulation and is associated with a restricted Ca^{2+} influx during the first AP accompanied by a build up in presynaptic Ca^{2+} concentration and, thus, an increase in the synaptic release probability once the second AP reaches the presynaptic terminal (Thomson, 2000; Zucker and Regehr, 2002). To analyze whether the increase in PPR in the presence of $Ca_v\beta_{4b}$ subunits could

account for a reduction in channel opening caused by $Ca_v\beta_{4b}$, we examined the possibility of detecting differences in the amount of channels opened by a hippocampal AP. We could not detect substantial differences between the $Ca_v\beta$-assembled channels during the paired-pulse protocol used. To provide an explanation for the facilitation behavior of $Ca_v\beta_{4b}$-expressing synapses, we analyzed several parameters, including Ca^{2+} dependence of the transmitter release, the effect of the expression of $Ca_v\beta$ subunits on the contribution of N- and P/Q-type channels to synaptic transmission, and somatic non–L-type currents. We found that the expression of $Ca_v\beta_{4b}$ changes the shape of the Ca^{2+} response curve, which is most likely not correlated with a change in the ratio between the P/Q- or N-type channel or a $Ca_v\beta_{4b}$ channel–specific effect on the terminal (Fig. S2, available at http://www.jcb.org/cgi/content/full/jcb.200702072/DC1). This result suggests that in the presence of $Ca_v\beta_{4b}$ subunits at the presynaptic terminal, the cooperativity of the Ca^{2+}- dependent transmitter release is changed. Recently, the cooperativity of the transmitter release was determined using the same rat hippocampal autapse system. The cooperativity was estimated to around 3 (Reid et al., 1998), a value which we determined and confirmed in our study of wild-type and $Ca_v\beta_{2a}$-expressing neurons. The authors did not find a difference in the contribution between N- or P/Q-type channels. This is important to note because $Ca_v\beta_4$ could preferentially assemble with one or the other channel type. For example, the preferential assembly with N- or P/Q-type channels would have important implications for the synaptic transmission at the calyx of Held, where N-type channels are suggested to be further apart from the release site than P/Q-type channels (Wu et al., 1999). The change in cooperativity in the presence of $Ca_v\beta_{4b}$ subunits may suggest that the coupling between the Ca^{2+} channels and the release machinery is affected or that the Ca^{2+} channels are more distant from the release site. The idea is supported by our finding that $Ca_v\beta_{4b}$-expressing neurons are more sensitive to the slow Ca^{2+} chelator EGTA. This is an important finding given the recent observation that the N terminus of the $Ca_v\beta_{4a}$ subunit can bind synaptotagmin and the microtubule-associated protein 1A (Vendel et al., 2006). This raises the possibility that the $Ca_v\beta_{4a}$ subunit is creating a $Ca_v\beta$ subunit–specific anchor between the Ca^{2+} channel and the synaptic release machinery (Weiss, 2006), whereas the $Ca_v\beta_{4b}$ subunit would not. Therefore, $Ca_v\beta_{4b}$ subunit–assembled channels might be further apart from the release machinery or may change the placement of the readily releasing vesicle next to the Ca^{2+} channels, which may cause the change in the Ca^{2+} response curve. In fact, it has been suggested recently that recruitment and placement of the synaptic vesicles to sites where Ca^{2+} channels cluster are important for rapid neurotransmitter release (Wadel et al., 2007).

Physiological consequences of neuronal Ca^{2+} channels assembled with different $Ca_v\beta$ subunits

$Ca_v\beta$ subunit–specific effects on synaptic transmitter release (i.e., facilitation and/or depression) will arise if a certain subunit is abundant in a neuronal circuit or synapse. For example, in the thalamus, a brain region that is critical for seizure activity, high expression levels of $Ca_v\beta_4$ subunits are found, whereas $Ca_v\beta_{1–3}$ subunits seem to be absent or at a lower abundance (Tanaka et al., 1995; Burgess and Noebels, 1999). Loss of $Ca_v\beta_4$ subunit function results in absence seizure epilepsy correlated with a reduced excitatory synaptic transmission in the thalamus (Caddick et al., 1999). $Ca_v\beta_2$ subunits have been suggested to play a crucial role for $Ca_v1.4$ function at the ribbon synapse of the outer plexiform layer of the retina, where these channels mediate glutamate release, whereas the role of $Ca_v\beta_2$ within the brain is poorly understood. Because $Ca_v\beta$ subunits are targets of protein phosphorylation and regulate the trafficking of the Ca^{2+} channels (Dolphin, 2003; Herlitze et al., 2003), it can be expected that activity-dependent trafficking of specific $Ca_v\beta$ subtypes in and out of synaptic terminals may occur as an important mechanism for the regulation of synaptic plasticity within a presynaptic terminal.

Materials and methods

Cell culture

Microisland and continental cultures of hippocampal neurons were prepared according to a modified version of published procedures (Bekkers and Stevens, 1991). In brief, hippocampal CA1-CA3 neurons from newborn rats (postnatal day 0–3) were enzymatically dissociated in 2 U/ml DME plus papain (Worthington) for 60 min at 37°C. Dissociated neurons were either plated onto astrocyte-covered poly-D-lysine/collagen (Sigma-Aldrich)-treated microislands that were prepared 3–5 d before plating (autaptic cultures) or were plated onto poly-D-lysine/collagen-treated coverslips that were placed invertly over astrocyte feeder cells (continental cultures). Neuronal cultures were grown in Neurobasal-A media (Invitrogen) supplemented with 4% B-27 (Invitrogen) and 2 mM Glutamax (Invitrogen) for 12–15 d.

Immunocytochemistry and imaging

Continental hippocampal cultures were prepared as described in the previous section and were infected with GFP-tagged $Ca_v\beta$ subunits. 12–18 h after infection, neurons were fixed with 4% PFA and permeabilized with 0.2% Triton X-100 in PBS. Anti–synaptobrevin-II (SYSY) and antisynapsin (Invitrogen) antibodies were used to label the synaptic markers. Neurons were incubated with the primary antibody overnight at 4°C, washed, and incubated with AlexaFluor568-conjugated secondary antibody (Invitrogen) for 30 min at room temperature. Cells were embedded in Prolong Gold Antifade (Invitrogen). Images were acquired with a confocal microscope (LSM 510; Carl Zeiss MicroImaging, Inc.) mounted on an inverted microscope (Axiovert 200M; Carl Zeiss MicroImaging, Inc.). Images were acquired with a 63× oil plan Apo NA 1.4 objective at room temperature, processed with the built-in LSM 510 software (version 3.5; Carl Zeiss MicroImaging, Inc.), and analyzed by using VOLOCITY software (Improvision).

Pan-β antibody

Polyclonal anti–pan-β antibody was raised by Harlan Bioproduct for Science according to a published procedure (Vance et al., 1998). In short, a highly conserved peptide sequence presented in all β subunits (CESYTSRPSDSDVSLEEDRE) was synthesized, and a standard 112-d protocol was used for polyclonal antibody production (Harlan Bioproduct for Science). The specificity of the product was documented with Western blots using rat brain homogenate as well as homogenates of HEK293 cells expressing $Ca_v\beta_{1b}$, $Ca_v\beta_2$, $Ca_v\beta_3$, or $Ca_v\beta_4$ subunit and resulted only in bands with desired molecular weights.

Electrophysiology and analysis

For HEK293 cell recordings, HEK293 cells (tsA201 cells) were transfected with the Ca^{2+} channel subunits $Ca_v\alpha_1 2.1$ and $Ca_v\alpha_2\delta$, with $Ca_v\beta_{1b}$, $Ca_v\beta_{2a}$, $Ca_v\beta_3$, or $Ca_v\beta_{4b}$, and with GFP to identify positively transfected cells (molar ratio of 2:1:1:0.25). Whole cell recordings were performed as described previously (Li et al., 2005). For EPSC recordings, only dots containing a single neuron forming excitatory synapses (autapses) were used using an EPC-9 amplifier (HEKA). Recordings were performed at room temperature.

For EPSC measurements as well as for recordings of Ca^{2+} currents in HEK293 cells, the extracellular recording solution contained 172 mM NaCl, 2.4 mM KCl, 10 mM Hepes, 10 mM glucose, 4 mM $CaCl_2$, and 4 $MgCl_2$, pH 7.3; the internal solution contained 145 mM potassium gluconate, 15 mM Hepes, 1 mM potassium-EGTA, 4 mM Na-ATP, and 0.4 mM Na-GTP, pH 7.3. For EGTA experiments (Fig. 9, E and F), the internal solution contained 10 mM potassium EGTA (Sigma-Aldrich), or 50 μM EGTA-AM (Invitrogen) was applied 15 min before recording to the extracellular recording solution. Currents were elicited by a 2-ms-long test pulse to 10 mV and recorded and analyzed as described previously (Wittemann et al., 2000). For recordings using various extracellular Ca^{2+} concentrations (extracellular $[Ca^{2+}]_o$), solutions containing different extracellular $[Ca^{2+}]_o$ were applied directly onto the recorded neurons by using a fast-flow perfusion system (ALA Scientific). Non–L-type channel recordings in cultured hippocampal neurons were performed as previously described (Li et al., 2005; Han et al., 2006). The internal recording solution contained 120 mM *N*-methyl-D-glucamine, 20 mM tetraethylammonium-Cl^-, 10 mM Hepes, 1 mM $CaCl_2$, 14 mM phosphocreatine (Tris), 4 mM Mg-ATP, 0.3 mM Na_2GTP, and 11 mM EGTA, pH 7.2, with methanesulfonic acid. The external solution contained 145 mM tetraethylammonium, 10 mM Hepes, 10 mM $CaCl_2$, and 15 mM glucose, pH 7.4, with methanesulfonic acid. In addition, 1 μM tetrodotoxin (Sigma-Aldrich) and 5 μM nimodipine (Sigma-Aldrich) were added to the external solution to block voltage-dependent Na^+ channels and L-type Ca^{2+} channels. Non–L-type currents were elicited by 500-ms voltage clamp ramps from –60 to 90 mV with 1-min intervals and by 100-ms-long voltage pulses from −60 to 0 mV (Fig. 6 B). Here, capacitative and tail currents were subtracted after the experiment. The sizes of RRPs were measured according to published procedures (Rosenmund and Stevens, 1996; Han et al., 2006). In short, 500 mM sucrose was applied directly onto the recorded autaptic neurons for 4 s by using a fast-flow perfusion system (ALA Scientific). The EPSC and RRP charge was calculated by integrating the currents elicited by the single AP or the sucrose application.

The asynchronous and phasic release was calculated as described in Otsu et al. (2004). In brief, we estimated the phasic release by integrating the EPSC after each pulse within the 20-Hz stimulation protocol after subtraction of a baseline value measured 1 ms before each test pulse. The asynchronous release was calculated by subtracting the phasic release from the total integrated current for each EPSC. The holding current was subtracted before integration in every experiment. Statistical significance throughout the experiments was evaluated with analysis of variance using Igor Pro software (Wavemetrics). Standard errors are mean ± SEM.

Quantitative real-time PCR

10^7 cells of acutely dissociated hippocampal neurons were plated on poly-D-lysine–collagen–coated plates for continental culture as described in the Cell culture section. The total RNA was subtracted from 14-d in vitro–cultured neurons with the RNeasy Mini kit (QIAGEN) and purified with on-column DNase digestion using the RNase-Free DNase Set (QIAGEN). For RT-PCR, 1 μg RNA was used for reverse transcription with the Advantage RT-for-PCR kit (BD Biosciences) to generate 100 μl cDNA, and 3 μl of the final RT product was used for real-time PCR of each $Ca_v\beta$ subunit. Real-time PCR quantification was performed on the iCycler Iq Detection System (Bio-Rad Laboratories) with CYBR green assay (Bio-Rad Laboratories). The DNA fragments of $Ca_v\beta_{1b}$, $Ca_v\beta_{2a}$, $Ca_v\beta_3$, and $Ca_v\beta_{4b}$ were amplified from cDNA with the following primer pairs: $Ca_v\beta_{1b}$ forward (GGCTGTGAGGTTGGTTTCAT) and $Ca_v\beta_{1b}$ backward (TGTCACCTGACTTGCTGGAG); $Ca_v\beta_2$ forward (CATGAGACCAGTGGTGTTGG) and $Ca_v\beta_2$ backward (CAGGGAGATGTCAGCAGTGA); $Ca_v\beta_3$ forward (CAGGTTTGATGGCAGGATCT) and $Ca_v\beta_3$ backward (GTGTCAGCATCCAACACCAC); $Ca_v\beta_4$ forward (GAGAGCGAAGTCCAAACCTG) and $Ca_v\beta_4$ backward (TCACCAGCCTTCCTATCCAC); and 18S forward (AAACGGCTACCACATCCAAG) and 18S backward (CCTCCAATGGATCCTCGTTA).

The specificity of RT-PCR products was documented with gel electrophoresis and resulted in a single product with desired length. The melt curve analysis showed that each primer pair had a single product-specific melting temperature. All primer pairs have at least 95% of PCR efficiency, as reported from the slopes of the standard curves generated by iQ software (version 3.1; Bio-Rad Laboratories). The PCR reactions used a modified two-step profile with initial denaturation for 3 min at 95°C, 40 cycles of 95°C for 15 s, and at 57°C for 25 s. Relative gene expression data were analyzed with the 2-ΔΔCT method (Livak and Schmittgen, 2001).

Electron microscopy

For immunoelectron microscopy of the cultured hippocampal neurons, 14-d in vitro neurons were infected with GFP-tagged $Ca_v\beta_{2a}$ or $Ca_v\beta_{4b}$ subunits with the Semliki Forest virus (SFV) expression system for 12 h before fixing with 4% PFA in 1× PBS for 20 min at 4°C. Cells were washed with 1× PBS containing 0.05% (vol/vol) Triton X-100, blocked with 10% goat serum (Invitrogen), and incubated with polyclonal rabbit anti-GFP antibody (Invitrogen) at 4°C overnight. The neurons were then rinsed five times with PBS/0.05% Triton X-100 for 3 min and incubated with goat anti–rabbit IgG conjugated with 10-nm gold particles (Electron Microscopy Sciences) for 2 h at room temperature on a shaker. After rinsing, neurons were fixed with 2% glutaraldehyde and 4% PFA in 0.1 M cacodylate buffer at 4°C overnight. After postfixing with 1% osmium tetroxide and staining with 1% uranyl acetate, neurons were dehydrated through an ethanol series from 50 to 100% ethanol and were transferred to propylene oxide, infiltrated with Embed 812 (Electron Microscopy Sciences) for 12 h, and hardened for 24 h at 60°C. Coverslips were removed, and 60-nm sections were cut on an ultramicrotome (Ultracut E; Reichert-Jung. The slices were recovered on Formvar-coated single slot copper grids and examined in a electronic microscope (JEM-1200EX; JEOL) at 80 kV.

For the brain slice immunoelectron microscopy, 100-nm-thick adult rat brain slices were prepared on a vibrating blade microtome (VT 1000S; Leica) and immediately infected with GFP-tagged $Ca_v\beta_{2a}$ or $Ca_v\beta_{4b}$ subunits with the SFV expression system for 12 h in an incubator with 5% CO_2 at 37°C. The expression of the subunits was verified by the GFP fluorescent signals before the slices were fixed with 4% PFA in 1× PBS at 4°C overnight. The slices were rinsed with 1× PBS containing 0.05% (vol/vol) Triton X-100 five times for 3 min, blocked with 10% goat serum (Invitrogen), and incubated with a polyclonal rabbit anti-GFP antibody (Invitrogen) overnight at 4°C. Procedures and conditions for the second antibody, postfixation, and embedding, etc., were the same as for cultured neurons.

cDNAs and virus production

Rat $Ca_v\beta_{1b}$, $Ca_v\beta_{2a}$, $Ca_v\beta_3$, and $Ca_v\beta_{4b}$ were gifts from T. Snutch (University of British Columbia, Vancouver, Canada) and E. Perez-Reyes (University of Virginia, Charlottesville, VA). They were cloned in frame into pEGFP-$C_{1–3}$ vectors (CLONTECH Laboratories, Inc.) and then into the Semliki forest virus vector pSFV1 (Life Technologies) for virus production. Thus, the GFP tag is located on the N terminus of the $Ca_v\beta$ subunits.

Membrane fractionation

About 8×10^6 hippocampal neurons were cultured on four collagen/poly-D-lysine–coated 100-mm culture dishes for 14 d and infected with GFP-tagged $Ca_v\beta_{1b}$, $Ca_v\beta_{2a}$, $Ca_v\beta_3$, and $Ca_v\beta_{4b}$ carrying virus for 13–16 h. Infected or noninfected cells were scraped in 0.32 M sucrose-TBS (0.15 M NaCl and 0.05 Tris, pH 7.4) containing 1× Complete Mini protease inhibitor (Roche) and were homogenized for 50 strokes with Dounce tissue grinder (Wheaton Millville) before promptly being loaded on top of freshly prepared 0.8 M/1.2 M sucrose-TBS gradient for centrifugation. Centrifugation was performed in a J-2-21 M/E ultracentrifuge (Beckman Coulter) at 3×10^4 rpm with a SW25.1 rotor for 45 min at 4°C. Equal volumes of the cytosol and membrane fractions were used for Western blots, which were performed according to standard procedures (Mark et al., 1995).

Online supplemental material

Fig. S1 shows that the AP amplitude during 20-Hz stimulations is not reduced in noninfected or $Ca_v\beta_{2a}$ and $Ca_v\beta_{4b}$ subunits expressing hippocampal neurons. Fig. S2 shows that $Ca_v\beta$ subunits expressed in hippocampal neurons do not change the relative contribution of N- and P/Q-type channels to non–L-type currents and EPSCs. Fig. S3 shows that the N terminus of $Ca_v\beta_{4b}$ interferes with synaptic transmitter release in hippocampal neurons. Online supplemental material is available at http://www.jcb.org/cgi/content/full/jcb.200702072/DC1.

We would like to thank Dr. L. Landmesser for reading the manuscript, Drs. L. Landmesser, R. Miller, and A. Malouf for helpful discussions, and Dr. R. Miller for help with the immunoelectron microscopy.

This work was supported by National Institutes of Health grants NS0447752 and NS42623 to S. Herlitze.

Submitted: 12 December 2006
Accepted: 29 June 2007

References

Ahmari, S.E., J. Buchanan, and S.J. Smith. 2000. Assembly of presynaptic active zones from cytoplasmic transport packets. *Nat. Neurosci.* 3:445–451.

Atluri, P.P., and W.G. Regehr. 1998. Delayed release of neurotransmitter from cerebellar granule cells. *J. Neurosci.* 18:8214–8227.

Bekkers, J.M., and C.F. Stevens. 1991. Excitatory and inhibitory autaptic currents in isolated hippocampal neurons maintained in cell culture. *Proc. Natl. Acad. Sci. USA*. 88:7834–7838.

Berggren, P.O., S.N. Yang, M. Murakami, A.M. Efanov, S. Uhles, M. Kohler, T. Moede, A. Fernstrom, I.B. Appelskog, C.A. Aspinwall, et al. 2004. Removal of Ca2+ channel beta3 subunit enhances Ca2+ oscillation frequency and insulin exocytosis. *Cell*. 119:273–284.

Bichet, D., V. Cornet, S. Geib, E. Carlier, S. Volsen, T. Hoshi, Y. Mori, and M. De Waard. 2000. The I-II loop of the Ca2+ channel alpha1 subunit contains an endoplasmic reticulum retention signal antagonized by the beta subunit. *Neuron*. 25:177–190.

Bogdanov, Y., N.L. Brice, C. Canti, K.M. Page, M. Li, S.G. Volsen, and A.C. Dolphin. 2000. Acidic motif responsible for plasma membrane association of the voltage-dependent calcium channel beta1b subunit. *Eur. J. Neurosci.* 12:894–902.

Brody, D.L., and D.T. Yue. 2000. Release-independent short-term synaptic depression in cultured hippocampal neurons. *J. Neurosci.* 20:2480–2494.

Burgess, D.L., and J.L. Noebels. 1999. Voltage-dependent calcium channel mutations in neurological disease. *Ann. NY Acad. Sci.* 868:199–212.

Caddick, S.J., C. Wang, C.F. Fletcher, N.A. Jenkins, N.G. Copeland, and D.A. Hosford. 1999. Excitatory but not inhibitory synaptic transmission is reduced in lethargic (Cacnb4(lh)) and tottering (Cacna1atg) mouse thalami. *J. Neurophysiol.* 81:2066–2074.

Catterall, W.A. 2000. Structure and regulation of voltage-gated Ca2+ channels. *Annu. Rev. Cell Dev. Biol.* 16:521–555.

Chen, Y.H., M.H. Li, Y. Zhang, L.L. He, Y. Yamada, A. Fitzmaurice, Y. Shen, H. Zhang, L. Tong, and J. Yang. 2004. Structural basis of the alpha1-beta subunit interaction of voltage-gated Ca2+ channels. *Nature*. 429:675–680.

Chien, A.J., T. Gao, E. Perez-Reyes, and M.M. Hosey. 1998. Membrane targeting of L-type calcium channels. Role of palmitoylation in the subcellular localization of the beta2a subunit. *J. Biol. Chem.* 273:23590–23597.

Dolphin, A.C. 2003. Beta subunits of voltage-gated calcium channels. *J. Bioenerg. Biomembr.* 35:599–620.

Fellin, T., S. Luvisetto, M. Spagnolo, and D. Pietrobon. 2004. Modal gating of human CaV2.1 (P/Q-type) calcium channels: II. the b mode and reversible uncoupling of inactivation. *J. Gen. Physiol.* 124:463–474.

Han, J., M.D. Mark, X. Li, M. Xie, S. Waka, J. Rettig, and S. Herlitze. 2006. RGS2 determines short-term synaptic plasticity in hippocampal neurons by regulating Gi/o mediated inhibition of presynaptic Ca^{2+} channels. *Neuron*. 51:575–586.

Hanlon, M.R., N.S. Berrow, A.C. Dolphin, and B.A. Wallace. 1999. Modelling of a voltage-dependent Ca2+ channel beta subunit as a basis for understanding its functional properties. *FEBS Lett.* 445:366–370.

Herlitze, S., and M.D. Mark. 2005. Distribution and targeting mechanisms of voltage activated Ca2+ channels. *In* Voltage-Gated Calcium Channels. G.W. Zamponi, editor. Kluwer Academic/Plenum Publishing Corp., New York. 113–40.

Herlitze, S., D.E. Garcia, K. Mackie, B. Hille, T. Scheuer, and W.A. Catterall. 1996. Modulation of Ca2+ channels by G-protein beta gamma subunits. *Nature*. 380:258–262.

Herlitze, S., G.H. Hockerman, T. Scheuer, and W.A. Catterall. 1997. Molecular determinants of inactivation and G protein modulation in the intracellular loop connecting domains I and II of the calcium channel alpha1A subunit. *Proc. Natl. Acad. Sci. USA*. 94:1512–1516.

Herlitze, S., H. Zhong, T. Scheuer, and W.A. Catterall. 2001. An allosteric mechanism for modulation of Ca2+ channels by G proteins, voltage-dependent facilitation, protein kinase C, and Cavb subunits. *Proc. Natl. Acad. Sci. USA*. 98:4699–4704.

Herlitze, S., M. Xie, J. Jan, A. Hümmer, K.V. Melnik-Martinez, R.L. Moreno, and M.D. Mark. 2003. Targeting mechanisms of high voltage-activated Ca2+ channels. *J. Bioenerg. Biomembr.* 35:621–637.

Hibino, H., R. Pironkova, O. Onwumere, M. Rousset, P. Charnet, A.J. Hudspeth, and F. Lesage. 2003. Direct interaction with a nuclear protein and regulation of gene silencing by a variant of the Ca2+-channel beta 4 subunit. *Proc. Natl. Acad. Sci. USA*. 100:307–312.

Li, X., A. Hummer, J. Han, M. Xie, K. Melnik-Martinez, R.L. Moreno, M. Buck, M.D. Mark, and S. Herlitze. 2005. G protein beta2 subunit-derived peptides for inhibition and induction of G protein pathways. Examination of voltage-gated Ca2+ and G protein inwardly rectifying K+ channels. *J. Biol. Chem.* 280:23945–23959.

Livak, K.J., and T.D. Schmittgen. 2001. Analysis of relative gene expression data using real-time quantitative PCR and the 2(-Delta Delta C(T)) Method. *Methods*. 25:402–408.

Luvisetto, S., T. Fellin, M. Spagnolo, B. Hivert, P.F. Brust, M.M. Harpold, K.A. Stauderman, M.E. Williams, and D. Pietrobon. 2004. Modal gating of human CaV2.1 (P/Q-type) calcium channels: I. The slow and the fast gating modes and their modulation by β subunits. *J. Gen. Physiol.* 124:445–461.

Mark, M.D., Y. Liu, S.T. Wong, T.R. Hinds, and D.R. Storm. 1995. Stimulation of neurite outgrowth in PC12 cells by EGF and KCl depolarization: a Ca(2+)-independent phenomenon. *J. Cell Biol.* 130:701–710.

Mark, M.D., S. Wittemann, and S. Herlitze. 2000. G protein modulation of recombinant P/Q-type calcium channels by regulators of G protein signalling proteins. *J. Physiol.* 528:65–77.

Maximov, A., and I. Bezprozvanny. 2002. Synaptic targeting of N-type calcium channels in hippocampal neurons. *J. Neurosci.* 22:6939–6952.

McGee, A.W., D.A. Nunziato, J.M. Maltez, K.E. Prehoda, G.S. Pitt, and D.S. Bredt. 2004. Calcium channel function regulated by the SH3-GK module in beta subunits. *Neuron*. 42:89–99.

Opatowsky, Y., C.C. Chen, K.P. Campbell, and J.A. Hirsch. 2004. Structural analysis of the voltage-dependent calcium channel beta subunit functional core and its complex with the alpha 1 interaction domain. *Neuron*. 42:387–399.

Otsu, Y., V. Shahrezaei, B. Li, L.A. Raymond, K.R. Delaney, and T.H. Murphy. 2004. Competition between phasic and asynchronous release for recovered synaptic vesicles at developing hippocampal autaptic synapses. *J. Neurosci.* 24:420–433.

Reid, C.A., J.M. Bekkers, and J.D. Clements. 1998. N- and P/Q-type Ca2+ channels mediate transmitter release with a similar cooperativity at rat hippocampal autapses. *J. Neurosci.* 18:2849–2855.

Richards, M.W., A.J. Butcher, and A.C. Dolphin. 2004. Ca2+ channel beta-subunits: structural insights AID our understanding. *Trends Pharmacol. Sci.* 25:626–632.

Rosenmund, C., and C.F. Stevens. 1996. Definition of the readily releasable pool of vesicles at hippocampal synapses. *Neuron*. 16:1197–1207.

Rousset, M., T. Cens, and P. Charnet. 2005. Alone at last! New functions for Ca2+ channel beta subunits? *Sci. STKE*. doi:10.1126/stke.2752005pe11.

Shapira, M., R.G. Zhai, T. Dresbach, T. Bresler, V.I. Torres, E.D. Gundelfinger, N.E. Ziv, and C.C. Garner. 2003. Unitary assembly of presynaptic active zones from Piccolo-Bassoon transport vesicles. *Neuron*. 38:237–252.

Stea, A., W.J. Tomlinson, T.W. Soong, E. Bourinet, S.J. Dubel, S.R. Vincent, and T.P. Snutch. 1994. Localization and functional properties of a rat brain alpha 1A calcium channel reflect similarities to neuronal Q- and P-type channels. *Proc. Natl. Acad. Sci. USA*. 91:10576–10580.

Stevens, C.F., and J.F. Wesseling. 1998. Activity-dependent modulation of the rate at which synaptic vesicles become available to undergo exocytosis. *Neuron*. 21:415–424.

Tanaka, O., H. Sakagami, and H. Kondo. 1995. Localization of mRNAs of voltage-dependent Ca(2+)-channels: four subtypes of alpha 1- and beta-subunits in developing and mature rat brain. *Brain Res. Mol. Brain Res.* 30:1–16.

Thomson, A.M. 2000. Facilitation, augmentation and potentiation at central synapses. *Trends Neurosci.* 23:305–312.

Tottene, A., T. Fellin, S. Pagnutti, S. Luvisetto, J. Striessnig, C. Fletcher, and D. Pietrobon. 2002. Familial hemiplegic migraine mutations increase Ca(2+) influx through single human CaV2.1 channels and decrease maximal CaV2.1 current density in neurons. *Proc. Natl. Acad. Sci. USA*. 99:13284–13289.

Van Petegem, F., K.A. Clark, F.C. Chatelain, and D.L. Minor Jr. 2004. Structure of a complex between a voltage-gated calcium channel beta-subunit and an alpha-subunit domain. *Nature*. 429:671–675.

Vance, C.L., C.M. Begg, W.L. Lee, H. Haase, T.D. Copeland, and M.W. McEnery. 1998. Differential expression and association of calcium channel alpha1B and beta subunits during rat brain ontogeny. *J. Biol. Chem.* 273:14495–14502.

Vendel, A.C., M.D. Terry, A.R. Striegel, N.M. Iverson, V. Leuranguer, C.D. Rithner, B.A. Lyons, G.E. Pickard, S.A. Tobet, and W.A. Horne. 2006. Alternative splicing of the voltage-gated Ca2+ channel beta4 subunit creates a uniquely folded N-terminal protein binding domain with cell-specific expression in the cerebellar cortex. *J. Neurosci.* 26:2635–2644.

Wadel, K., E. Neher, and T. Sakaba. 2007. The coupling between synaptic vesicles and Ca(2+) channels determines fast neurotransmitter release. *Neuron*. 53:563–575.

Weiss, N. 2006. The calcium channel beta4a subunit: a scaffolding protein between voltage-gated calcium channel and presynaptic vesicle-release machinery? *J. Neurosci.* 26:6117–6118.

Wittemann, S., M.D. Mark, J. Rettig, and S. Herlitze. 2000. Synaptic localization and presynaptic function of calcium channel beta 4-subunits in cultured hippocampal neurons. *J. Biol. Chem.* 275:37807–37814.

Wu, L.G., R.E. Westenbroek, J.G.G. Borst, W.A. Catterall, and B. Sakmann. 1999. Calcium channel types with distinct presynaptic localization couple differentially to transmitter release in single calyx-type synapses. *J. Neurosci.* 19:726–736.

Xu, J., and L.G. Wu. 2005. The decrease in the presynaptic calcium current is a major cause of short-term depression at a calyx-type synapse. *Neuron*. 46:633–645.

Zucker, R.S., and W.G. Regehr. 2002. Short-term synaptic plasticity. *Annu. Rev. Physiol.* 64:355–405.